Divergent features of the coenzyme Q:cytochrome *c* oxidoreductase complex in *Toxoplasma gondii* parasites

Jenni A. Hayward[1], Esther Rajendran[1], Soraya M. Zwahlen[1], Pierre Faou[2], Giel G. van Dooren[1,*]

[1]Research School of Biology, Australian National University, Canberra, ACT, Australia

[2]Department of Biochemistry and Genetics, La Trobe Institute for Molecular Science, La Trobe University, Victoria, Australia

Running Title: Divergent Complex III in *Toxoplasma* parasites

* Corresponding author

E-mail: giel.vandooren@anu.edu.au

Abstract

The mitochondrion is critical for the survival of apicomplexan parasites. Several major anti-parasitic drugs, such as atovaquone and endochin-like quinolones, act through inhibition of the mitochondrial electron transport chain at the coenzyme Q:cytochrome *c* oxidoreductase complex (Complex III). Despite being an important drug target, the protein composition of Complex III of apicomplexan parasites has not been elucidated. Here, we undertake a mass spectrometry-based proteomic analysis of Complex III in the apicomplexan *Toxoplasma gondii*. Along with canonical subunits that are conserved across eukaryotic evolution, we identify several novel or highly divergent Complex III components that are conserved within the apicomplexan lineage. We demonstrate that one such subunit, which we term *Tg*QCR11, is critical for parasite proliferation, mitochondrial oxygen consumption and Complex III activity, and establish that loss of this protein leads to defects in Complex III integrity. We conclude that the protein composition of Complex III in apicomplexans differs from that of the mammalian hosts that these parasites infect.

Author summary

Apicomplexan parasites cause numerous diseases in humans and animals, including malaria (*Plasmodium* species) and toxoplasmosis (*Toxoplasma gondii*). The coenzyme Q:cytochrome *c* oxidoreductase protein complex (Complex III) performs a central role in the mitochondrial electron transport chain of many eukaryotes. Despite being the target of several major anti-apicomplexan drugs, the protein composition of Complex III in apicomplexans was previously unknown. Our work identifies novel proteins in Complex III of apicomplexans, one of which is critical for complex function and integrity. Our study highlights divergent features of Complex III in apicomplexans, and provides a broader understanding of Complex III evolution in eukaryotes. Our study also provides important insights into what sets this major drug target apart from the equivalent complex in host species.

Introduction

Apicomplexans are a large phylum of intracellular, protozoan parasites that include the causative agents of malaria (*Plasmodium* species) and toxoplasmosis (*Toxoplasma gondii*). These parasites impose major economic and health burdens on human societies, and, in the absence of effective vaccines [1, 2], there is a heavy reliance on drugs to treat disease. The parasite coenzyme Q:cytochrome *c* oxidoreductase complex (Complex III of the mitochondrial electron transport chain, ETC) represents one of the major drug targets in these parasites [3, 4]. Numerous inhibitors of Complex III, including atovaquone and endochin-like quinolones, are in clinical use or in preclinical development against apicomplexans [5-7].

The ETC consists of a series of protein complexes that are embedded in the inner mitochondrial membrane. Electrons derived from the oxidation of mitochondrial substrates are donated via the action of dehydrogenases to a mobile electron carrier in the inner membrane called coenzyme Q (CoQ). CoQ exchanges electrons with the coenzyme Q:cytochrome *c* oxidoreductase complex (Complex III). Here, electrons from CoQ are donated to the cytochrome *b* protein of Complex III, from where they are either donated on to cytochrome *c*, a mobile carrier protein in the mitochondrial intermembrane space, or donated back to CoQ in a process called the Q cycle [8]. The transfer of electrons to cytochrome *c* occurs via an iron-sulfur cluster and a heme prosthetic group in the Rieske and cytochrome c_1 proteins of Complex III, respectively. Electrons from cytochrome *c* are transported on to the cytochrome *c* reductase complex (Complex IV), which facilitates electron transfer to the terminal electron acceptor, oxygen [9]. Electron transport through Complexes III and IV is coupled to the translocation of protons from the mitochondrial matrix into the intermembrane space, thereby generating a proton motive force across the inner membrane.

This proton gradient is used for several important mitochondrial processes, including protein and solute import, and driving the activity of ATP synthase (Complex V) to generate ATP [10].

It is becoming increasingly apparent that the ETC of myzozoans – a eukaryotic lineage that includes apicomplexan parasites and their closest free living relatives, two phyla of marine algae called chromerids and dinoflagellates – differs considerably from that of other eukaryotes, including the animal hosts that apicomplexans infect [11-13]. For instance, Complexes IV and V from these organisms contain many subunits that lack homologs outside the myzozoan lineage [14-16]. Uncovering such diversity in a canonical mitochondrial process is of interest from both an evolutionary and a therapeutic standpoint. Evolutionarily, these studies provide insights into the diversification of mitochondria since eukaryote lineages diverged from their common ancestor >1.5 billion years ago [17]. Therapeutically, the discovery of novel proteins in a critical pathway such as the ETC opens avenues for drug development.

Despite being a major drug target, many important features of Complex III in these parasites, including its protein composition, have not yet been elucidated. Here, we undertake a proteomic analysis of Complex III in *T. gondii*. Along with canonical subunits that are conserved in host organisms, we identified two highly divergent and two novel, apicomplexan-specific Complex III components. We demonstrate that one of the apicomplexan-specific subunits, which we term *Tg*QCR11, is critical for parasite proliferation and ETC function through maintaining Complex III integrity. We conclude that Complex III of apicomplexans contains highly divergent and novel protein subunits, and differs considerably from the equivalent complex in animal hosts.

Results

***T. gondii* Complex III contains both canonical and novel protein subunits.** The putative mitochondrial processing peptidase alpha subunit (*Tg*MPPα; www.toxodb.org gene ID TGGT1_202680) was shown previously to localize to the mitochondrion of *T. gondii* [18]. In many other eukaryotes, the MPPα protein functions in both the cleavage of mitochondrial-targeting pre-sequences from mitochondrial matrix proteins as they are imported into the mitochondrion, and as one of the so-called Core proteins of Complex III [19]. To facilitate further characterization of *Tg*MPPα, we introduced a TEV-HA tag into the 3' end of the open reading frame of the native *Tg*MPPα locus in *T. gondii* parasites (Fig. S1). To determine whether *Tg*MPPα exists as part of a protein complex, we extracted proteins from *Tg*MPPα-TEV-HA parasites using either 1% (v/v) Triton X-100, 1% (w/v) n-Dodecyl β-D-maltoside (DDM) or 1% (w/v) digitonin detergents, and separated solubilized protein complexes by blue native (BN)-PAGE. Western blotting with anti-HA antibodies revealed that the primary *Tg*MPPα-TEV-HA complex is ~675 kDa in mass when solubilized in all three detergents (Fig. 1A), though a fainter secondary complex at ~220 kDa was also observed. By contrast, the molecular mass of *Tg*MPPα-TEV-HA when separated by SDS-PAGE was ~60 kDa (Fig. 1B). We conclude that *Tg*MPPα is a component of a ~675 kDa protein complex.

To identify the proteins that comprise the *Tg*MPPα-containing complex, we immunoprecipitated *Tg*MPPα-TEV-HA and associated proteins, then subjected the sample to mass spectrometry-based proteomic analysis. As a control for these experiments, we purified the unrelated cytochrome *c* oxidase complex (Complex IV of the ETC). To purify Complex IV, we introduced a TEV-HA tag into the 3' end of the cytochrome c oxidase subunit 2a (*Tg*Cox2a; TGGT1_226590) open reading frame (Fig. S1), immunoprecipitated *Tg*Cox2a-TEV-HA and associated proteins, and performed a

separate mass spectrometry-based proteomic analysis. Using this approach, we identified five proteins – including *Tg*MPPα – that were enriched in the *Tg*MPPα-TEV-HA immunoprecipitation compared to the *Tg*Cox2a-TEV-HA immunoprecipitation across three independent experiments (Fig. 1C, D; Table S1). All five proteins are annotated as canonical components of Complex III, including the Core/mitochondrial processing peptidase protein *Tg*MPPβ (TGGT1_236210), the iron-sulfur cluster protein *Tg*Rieske (TGGT1_320220), the so-called '14 kDa' protein *Tg*QCR7 (TGGT1_288750), and the cytochrome c_1 heme protein *Tg*CytC1 (TGGT1_246540). Two other canonical Complex III proteins – the 'hinge' protein TgQCR6 (TGGT1_320140) and the cytochrome *b* protein (*Tg*CytB; TGGT1_362110) – were highly enriched in the *Tg*MPPα immunoprecipitation but excluded from the initial analysis because they were absent from at least one replicate of the *Tg*Cox2a control (Fig. 1D; Table S1). Note that the gene ID for *Tg*CytB (TGGT1_362110) encodes a truncated protein, and may represent one of several fragmented *Tg*CytB pseudogenes encoded by genetic material that occurs as 'junk' DNA in the nuclear genome of *T. gondii*, rather than the actual mitochondrial genome-encoded *Tg*CytB gene [20, 21].

Given that two canonical Complex III proteins were excluded from the initial analysis, we reasoned that a more comprehensive assessment of the data might reveal additional subunits that were likewise excluded. We shortlisted six additional proteins that were highly enriched in all three *Tg*MPPα replicates relative to *Tg*Cox2a (either absent from all *Tg*Cox2a samples or > 100-fold more abundant in the *Tg*MPPα purification than in the *Tg*Cox2a purification) (Fig. 1D; Table S1). Of these six proteins, five were annotated as hypothetical proteins (TGGT1_201880, TGGT1_227910, TGGT1_207170, TGGT1_214250, and TGGT1_242780) and one was annotated as a GAF domain-containing protein (TGGT1_270800). We utilized Localization of Organelle Proteins by Isotope Tagging ("LOPIT") cellular localization data [13] coupled with our previously

published mitochondrial proteome [15] to assess whether these proteins are likely to be mitochondrial. All the proteins were identified in both the mitochondrial proteome and the mitochondrial membrane fraction of the "LOPIT" dataset, with the exception of TGGT1_242780, which we excluded from further consideration (Fig. 1D, gray).

We employed a phylogenomic approach to further assess the candidate Complex III proteins. The chromerid *Vitrella brassicaformis* contains the full suite of ETC complexes including Complex III, while *Chromera velia* lacks Complex III but retains the other ETC complexes [12]. We reasoned that if a protein has a homolog in *V. brassicaformis* but not in *C. velia*, this would support the hypothesis that it is a Complex III subunit. In addition, the apicomplexan *Cryptosporidium parvum* contains highly reduced mitochondria that lack Complex III [22]. We further hypothesized that 'true' Complex III proteins were likely to be absent from *C. parvum*. To this end, we performed tBLASTn searches of EuPathDB using the identified proteins as queries to identify homologs in *Plasmodium falciparum*, *V. brassicaformis, C. velia* and *C. parvum* (Fig. 1D). Since *Tg*MPPα and *Tg*MPPβ function together as a mitochondrial peptidase protein complex, potentially separate from their function in Complex III, it is unsurprising that these proteins are found in all four species (Fig. 1D). In contrast, most other canonical Complex III proteins have homologs in *P. falciparum* and *V. brassicaformis* but not in *C. velia* and *C. parvum.* An interesting exception is the *Tg*Rieske protein, which has a homolog in *C. velia* (Fig. 1D). The *Cv*Rieske protein lacks the long N-terminus typical of other Rieske proteins, but retains the iron-sulfur cluster-containing core, implying this protein may have a secondary function in *C. velia*. A potential *Tg*CytC1 homolog was also identified in *C. velia* (Fig. 1D); however, this matched only to the N-terminus of *Tg*CytC1, and lacked key resides including those that mediate heme binding. The *Cv*CytC1 is likely not a functional CytC1 protein.

Of the additional proteins that we shortlisted, one has homologs in both chromerids (TGGT1_270800) and was therefore excluded from further analysis, three have homologs in *V. brassicaformis* but not *C. velia* (TGGT1_201880, TGGT1_227910, TGGT1_214250), and one appeared to be restricted to *T. gondii* (TGGT1_207170) (Fig. 1D). Further analysis of TGGT1_207170 using iterative JackHMMER homology searches identified a homolog of this protein in *P. falciparum* and numerous other apicomplexans, but not in *C. parvum*, chromerids or dinoflagellates (Fig. 1D). These data suggest that TGGT1_207170 may be an apicomplexan-specific protein.

To investigate whether the four shortlisted proteins (Fig. 1D, green) have any similarity to known Complex III proteins, we queried each protein against the Protein Data Bank (PDB) using HHPRED, a profile hidden Markov model search tool designed to identify homologous proteins with limited sequence similarity [23]. This analysis predicted that TGGT1_227910 has homology to the yeast Complex III protein QCR8 and TGGT1_201880 has homology to yeast QCR9. We therefore termed these two divergent Complex III subunits *Tg*QCR8 and *Tg*QCR9, respectively (Fig. 1D; Fig. S2; Fig S3). The remaining two proteins were not matched to proteins from PDB with any confidence. In total, our proteomic analysis identified *T. gondii* homologs to nine out of the ten proteins from the well-studied Complex III of budding yeast, with no homolog to the yeast QCR10 protein apparent in *T. gondii*. In addition, we identified two proteins that were restricted to the myzozoan or apicomplexan lineages. We termed these protein *Tg*QCR11 (TGGT1_214250) and *Tg*QCR12 (TGGT1_207170), delineating them from the 10 "QCR" protein from yeast (Fig. 1D; Fig. S4; Fig S5). All the candidate Complex III proteins that were tested in a genome-wide CRISPR screen were predicted to be important for growth of the tachyzoite stage of *T. gondii* [24] (Fig. 1D).

To begin to characterize the candidate Complex III proteins experimentally, we introduced FLAG epitope tags into the 3' end of the open reading frames of the *Tg*QCR8, *Tg*QCR9, *Tg*QCR11, and *Tg*QCR12 loci in an existing *Tg*MPPα-HA background strain [18] (Fig. S6). We then undertook western blot analysis and immunofluorescence assays to analyze the expression and cellular localization of these proteins. All four proteins were found to be between 15-20 kDa in mass and to localize to the mitochondrion (Fig. 2). Interestingly, the relative abundance of these four proteins appeared to differ, with *Tg*QCR11-FLAG and *Tg*QCR8-FLAG the most abundant and *Tg*QCR12-FLAG the least (Fig. S7).

We next sought to determine whether *Tg*QCR11-FLAG, *Tg*QCR8-FLAG, *Tg*QCR9-FLAG and *Tg*QCR12-FLAG exist in protein complexes. To do this, we extracted proteins from the four parasite lines and from the *Tg*MPPα-TEV-HA parasite line using 1% (w/v) DDM and separated proteins by BN-PAGE. Western blotting using anti-FLAG antibodies revealed that all four proteins exist in a protein complex of ~675 kDa, approximately the same mass as the *Tg*MPPα-TEV-HA complex when an adjacent lane run on the same gel was probed with anti-HA antibodies (Fig. 3A).

As a direct test for whether *Tg*QCR11-FLAG, *Tg*QCR8-FLAG, *Tg*QCR9-FLAG and *Tg*QCR12-FLAG proteins are part of the same protein complex as *Tg*MPPα-HA, we performed co-immunoprecipitation experiments. Immunoprecipitation of *Tg*MPPα-HA with anti-HA antibodies co-purified each of the four FLAG-tagged proteins, but not the unrelated mitochondrial protein *Tg*Tom40 (Fig. 3B-E). Likewise, immunoprecipitation of *Tg*QCR11-FLAG (Fig. 3B), *Tg*QCR8-FLAG (Fig. 3C), *Tg*QCR9-FLAG (Fig. 3D) and *Tg*QCR12-FLAG (Fig. 3E) with anti-FLAG antibodies co-purified *Tg*MPPα-HA but not *Tg*Tom40. In all instances, we identified a small proportion of *Tg*MPPα-HA in the unbound fraction of the anti-FLAG immunoprecipitations (Fig. 3B-D). This could represent the ~220 kDa complex observed for *Tg*MPPα-HA in BN-PAGE that

196 is absent from the BN-PAGE analyses of the other proteins (Fig. 3A). Together, these data indicate
197 that *Tg*MPPα-HA and the four QCR proteins exist in the same, ~675 kDa protein complex.

198 **_Tg_QCR11 is important for _T. gondii_ proliferation and mitochondrial oxygen consumption.**

199 The existence of *Tg*QCR11-FLAG, *Tg*QCR8-FLAG, *Tg*QCR9-FLAG and *Tg*QCR12-FLAG in a
200 complex with the core protein *Tg*MPPα-HA suggests that these proteins are components of
201 Complex III in *T. gondii*. To elucidate the importance and role of one of the apicomplexan-specific
202 Complex III proteins, we undertook a functional characterization of *Tg*QCR11. We first added a
203 FLAG tag to the 3' end of the *Tg*QCR11 gene (Fig. S8A-B) and then replaced the native promoter
204 of *Tg*QCR11 with an anhydrotetracycline (ATc)-regulated promoter (Fig. S8C-D). We termed the
205 resultant ATc-regulated *Tg*QCR11 strain 'r*Tg*QCR11-FLAG'. We also added an HA tag to the 3'
206 end of the *Tg*MPPα gene in this strain (Fig. S8E-F), resulting in a strain we termed 'r*Tg*QCR11-
207 FLAG/*Tg*MPPα-HA'.

208 To examine the extent of *Tg*QCR11 knockdown upon the addition of ATc, we cultured r*Tg*QCR11-
209 FLAG/*Tg*MPPα-HA parasites in the absence of ATc or in the presence of ATc for 1-3 days, then
210 separated proteins by SDS-PAGE and performed western blotting. *Tg*QCR11-FLAG expression
211 levels decreased substantially upon the addition of ATc, with only a small amount of protein
212 detectable after 3 days in ATc (Fig. 4A). To investigate the impact of *Tg*QCR11-FLAG
213 knockdown on parasite proliferation, we grew wild type (WT) and r*Tg*QCR11-FLAG/*Tg*MPPα-
214 HA parasites in the absence or presence of ATc for 8 days and compared plaque sizes. Plaque sizes
215 in r*Tg*QCR11 but not WT parasites was severely impaired in the presence of ATc (Fig. 4B). To
216 determine whether this proliferation defect was specifically due to loss of *Tg*QCR11, we
217 complemented the r*Tg*QCR11-FLAG strain with an additional copy of *Tg*QCR11 expressed from
218 the constitutively expressed α-tubulin promoter. Complementation with constitutively expressed

219 *Tg*QCR11 restored plaque formation in r*Tg*QCR11 parasites cultured in the presence of ATc (Fig.
220 4B), indicating that the proliferation defect we observed upon *Tg*QCR11 knockdown was
221 specifically due to loss of *Tg*QCR11.

222 Oxygen acts as the final electron acceptor in the ETC. If *Tg*QCR11 is an important component of
223 Complex III, we hypothesized that knockdown of *Tg*QCR11 knockdown would lead to defects in
224 oxygen consumption in the parasite. To test this, we utilized a previously established assay to
225 measure parasite oxygen consumption using a Seahorse XFe96 extracellular flux analyzer [15].
226 We grew WT and r*Tg*QCR11-FLAG/*Tg*MPPα-HA parasites in the absence of ATc or in the
227 presence of ATc for 1-3 days then measured their basal mitochondrial oxygen consumption rate
228 (mOCR). While the presence of ATc did not impair basal mOCR in WT parasites, the basal mOCR
229 of r*Tg*QCR11-FLAG parasites was substantially depleted upon *Tg*QCR11 knockdown (Fig. 4C),
230 indicating that *Tg*QCR11 is important for mitochondrial oxygen consumption.

231 We wondered whether the severe deficiency in mOCR observed upon *Tg*QCR11 knockdown was
232 due to a specific defect in the ETC, or whether it was caused by a more general defect in
233 mitochondrial function or parasite viability. To test whether *Tg*QCR11 knockdown causes any
234 gross defects in mitochondrial morphology, we grew r*Tg*QCR11/*Tg*MPPα-HA parasites in the
235 absence or presence of ATc and performed immunofluorescence assays to visualize both the inner
236 (*Tg*MPPα-HA) and outer (*Tg*Tom40) mitochondrial membranes. This revealed no observable
237 defects in mitochondrial morphology upon *Tg*QCR11 knockdown (Fig. S9A). Next, we tested
238 whether parasites remain viable following knockdown of *Tg*QCR11. To do this, we pre-incubated
239 r*Tg*QCR11 parasites in the presence of ATc for 3 days (a time point when *Tg*QCR11 is knocked
240 down substantially and mOCR is minimal (Fig. 4)) and then set up plaque assays in the absence or
241 presence of ATc. After 8 days proliferation, we compared plaque size to parasites that had not been

pre-incubated in ATc. Plaque size and number were similar between the ATc-pre-incubated and non-pre-incubated parasites when grown in the absence of ATc, while parasites grown in ATc underwent minimal growth, regardless of whether they were pre-incubated with ATc (Fig. S9B). These results indicate that *Tg*QCR11 knockdown is reversible and that r*Tg*QCR11 parasites grown in ATc for 3 days have similar viability to parasites grown in the absence of ATc.

To observe what happens to other aspects of parasite metabolism upon *Tg*QCR11 knockdown, we measured the extracellular acidification rate (ECAR) of WT and r*Tg*QCR11 parasites grown in the absence or presence of ATc. We have previously used ECAR as a general indication of parasite metabolic activity [15, 25]. ECAR levels of WT and r*Tg*QCR11 parasites grown in the absence of ATc or WT parasites grown in the presence of ATc were not significantly different (Fig. 4D; Fig. S9C). By contrast, growth of r*Tg*QCR11 parasites in the presence of ATc for 2 days resulted in a significant *increase* in ECAR (Fig. 4D; Fig. S9C), indicating that parasites remained metabolically active upon *Tg*QCR11 knockdown. The small but significant increase in ECAR upon *Tg*QCR11 knockdown may indicate that the parasite compensates for loss of mOCR by upregulating other aspects of cellular metabolism (e.g. glycolysis), though this needs to be studied further.

Together, these data indicate that the defects observed in mitochondrial oxygen consumption upon *Tg*QCR11 knockdown were not due to general defects in mitochondrial morphology, parasite viability or cellular metabolism. We therefore conclude that *Tg*QCR11 has an important and specific role in the ETC of *T. gondii* parasites, consistent with its association with Complex III.

***Tg*QCR11 is important for the function and integrity of Complex III.**

To establish whether *Tg*QCR11 is important for Complex III function in *T. gondii*, we sought to undertake a more direct interrogation of the functionality of various ETC components upon

264 *Tg*QCR11 knockdown. To do this, we established an XFe96 flux analyzer-based assay that enabled
265 us to measure substrate-dependent mOCR using digitonin-permeabilized parasites. Permeabilizing
266 the plasma membrane of parasites with digitonin allows the passage of substrates with polar or
267 hydrophobic functional groups into parasites, where they can feed electrons into the ETC either
268 directly or via mitochondrial metabolism. Supplying different combinations of substrates and
269 inhibitors during the assay enables an assessment of the functionality of different ETC complexes
270 (Fig. 5A [26]).

271 We grew WT, r*Tg*QCR11 and r*Tg*ApiCox25 (an ATc-regulatable strain that enables knockdown
272 of the Complex IV protein *Tg*ApiCox25 [15]) parasites in the absence of ATc or in the presence
273 of ATc for 1-3 days. Parasites were starved for 1 hour in base media to deplete endogenous
274 substrates, and then permeabilized with 0.002% (w/v) digitonin. The five readings taken before
275 injection of substrate show that permeabilized parasites have very low OCR (Fig. 5B), indicating
276 that the 1 hour starvation successfully depleted endogenous substrates. Injection of the
277 tricarboxylic acid (TCA) cycle substrates malate and glutamate caused an almost instantaneous
278 increase in OCR in WT, r*Tg*QCR11 and r*Tg*ApiCox25 parasites that were cultured in the absence
279 of ATc (Fig. 5B). As this OCR could be abolished by subsequent injection of the Complex III
280 inhibitors antimycin A and atovaquone (Fig. 5B), these data indicate that the ETC is functional in
281 these parasites. The malate/glutamate-elicited mOCR of WT parasites grown for 3 days in the
282 presence of ATc was not significantly different to WT parasites grown in the absence of ATc (Fig.
283 5C), indicating that ATc itself does not impact ETC function. By contrast, knockdown of
284 *Tg*QCR11 and *Tg*ApiCox25 caused significant decreases in malate/glutamate-dependent mOCR
285 (Fig. 5C).

We next asked whether defects in malate/glutamate-dependent mOCR upon *Tg*QCR11 or *Tg*ApiCox25 knockdown occurred upstream or downstream of cytochrome *c*. To test this, we injected the cytochrome *c* substrate N,N,N′,N′-tetramethyl-p-phenylenediamine dihydrochloride (TMPD). Reduced TMPD donates electrons directly to cytochrome *c*, downstream of Complex III, and should therefore rescue mOCR in parasites with an ETC defect upstream of cytochrome *c* (Fig. 5A). By contrast, a Complex IV defect should not be rescued by TMPD since Complex IV is downstream of cytochrome *c*. Injection of TMPD caused an increase in mOCR in r*Tg*QCR11 parasites cultured in the presence of ATc (Fig. 5B). By contrast, r*Tg*ApiCox25 parasites cultured for 2 or 3 days on ATc had very little TMPD-dependent mOCR (Fig. 5B). Calculating the fold stimulation of mOCR by TMPD relative to malate/glutamate-dependent mOCR indicates that r*Tg*QCR11 parasites grown for 3 days on ATc have 10-fold greater stimulation of mOCR by TMPD relative to malate (Fig. 5D). This demonstrates that Complex IV activity is largely retained upon *Tg*QCR11 knockdown and implies that the defect in ETC activity upon loss of this protein occurs upstream of cytochrome *c*. By contrast, r*Tg*ApiCox25 parasites grown for 3 days on ATc have little stimulation of mOCR by TMPD relative to malate/glutamate, indicating that loss of *Tg*ApiCox25 leads to a defect in Complex IV activity (Fig. 5D).

The preceding data indicate that loss of *Tg*QCR11 leads to defects in the ETC upstream of cytochrome *c*. Since malate/glutamate can feed into the ETC via the TCA cycle [11, 27], it is conceivable that defects we observe in mOCR upon *Tg*QCR11 knockdown could be the result of defects in the TCA cycle rather than a selective defect in Complex III. To address this, we measured mOCR using the substrate glycerol 3-phosphate, which donates electrons to CoQ independently of the TCA cycle (Fig. 5A; [11, 27]). Knockdown of *Tg*QCR11 caused a similar decrease in glycerol 3-phosphate-dependent mOCR compared to malate/glutamate-dependent

mOCR (Fig. 5E, F). Since mOCR elicited by two different substrates, one of which is independent of the TCA cycle, was impaired by knockdown of *Tg*QCR11, we conclude that loss of *Tg*QCR11 likely leads to a selective defect in Complex III activity.

Given the severe defect in mOCR observed upon *Tg*QCR11 knockdown, we wondered whether the integrity of Complex III is compromised by loss of *Tg*QCR11. To assess this, we set out to measure the effects of *Tg*QCR11 knockdown on several Complex III proteins. First, we integrated TEV-HA tags into the 3' ends of the *Tg*QCR8 and *Tg*QCR12 open reading frames in the r*Tg*QCR11-FLAG parasite line (Fig. S10). We then grew r*Tg*QCR11-FLAG/MPPα-HA, r*Tg*QCR11-FLAG/*Tg*QCR8-HA and r*Tg*QCR11-FLAG/*Tg*QCR12-HA parasites in the absence of ATc or in the presence of ATc for 1-3 days and assessed Complex III integrity by BN-PAGE. Strikingly, the ~675 kDa complex of all three proteins was depleted upon *Tg*QCR11 knockdown (Fig. 6A-C), suggesting that Complex III assembly and/or stability may be impaired upon loss of *Tg*QCR11. We wondered whether the abundance of Complex III proteins may also be affected by *Tg*QCR11 knockdown, and assessed this by SDS-PAGE and western blotting. Interestingly, while the abundance of MPPα remained consistent (Fig. 6D), the abundance of *Tg*QCR12 and *Tg*QCR8 decreased by day 2-3 on ATc (Fig. 6E-F), suggesting that knockdown of *Tg*QCR11 decreases the abundance of some Complex III proteins but not others. It is possible that MPPα abundance remains unchanged because, in addition to being a component of Complex III, it exists in a lower mass, ~220 kDa complex that our BN-PAGE analysis indicated is retained upon *Tg*QCR11 knockdown (Fig. 6A), which could represent the mitochondrial processing peptidase in these parasites. Together, these data indicate that *Tg*QCR11 is a novel, myzozoan-specific subunit of Complex III in *T. gondii* that is critical for Complex III function by maintaining the integrity of this protein complex.

Discussion

In this study, we characterized Complex III of the mitochondrial ETC in *T. gondii* parasites, which we demonstrate exists as a ~675 kDa complex comprising 11 protein subunits (Fig.1). Our data are consistent with an independent, parallel study by MacLean and colleagues, who identified the same 11 subunits in a broader proteomic analysis of mitochondrial respiratory chain complexes in *T. gondii* (MacLean *et al*. BioRxiv, 2020). The number of subunits we identified in *T. gondii* Complex III is similar to that reported for bovine [28-30], yeast [31] and plants [19, 32] complexes (11, 10 and 10 subunits, respectively), and the mass is similar to the fully-assembled yeast complex (670 kDa; [33]). The overall architecture of Complex III in eukaryotes is broadly conserved as a homodimer, with one copy of each subunit per monomer [28-31, 34], and we would suspect that this is also the case for *T. gondii*. The sum of the predicted masses of the 11 *T. gondii* Complex III subunits is ~350 kDa (assuming *Tg*CytB mass to be ~41 kDa [20]), giving a mass of ~700 kDa for the Complex III homodimer, which is in the ballpark of the ~675 kDa we observed by BN-PAGE. A caveat to this conclusion is that we observed different abundances in some Complex III subunits (Fig. S7), raising the possibility that not all subunits exist in a strict 1:1 stoichiometry per monomer.

In our proteomic analysis of *T. gondii* Complex III, we identified numerous canonical subunits, including the three electron transporting subunits (*Tg*Rieske, *Tg*CytB and *Tg*CytC1), the two core proteins (*Tg*MPPα and *Tg*MPPβ), and two known additional (or so-called 'supernumerary') subunits, the 'hinge' protein *Tg*QCR6 and '14 kDa' protein *Tg*QCR7. Our analysis also identified two highly divergent supernumerary subunits, *Tg*QCR8 and *Tg*QCR9, which were only identifiable after considering the structural features of these proteins. This indicates that, like several supernumerary proteins in Complexes IV and V of *T. gondii* [14-16], the ~1.5 billion years

of evolution since the common ancestor of apicomplexans and other eukaryotes has resulted in considerable divergence in the sequences of these ETC proteins.

Intriguingly, our analysis also identified two novel Complex III subunits (*Tg*QCR11 and *Tg*QCR12) that are restricted to organisms closely related to *T. gondii*. *Tg*QCR11 has homologues in other myzozoans – a lineage which comprises apicomplexans, as well as their closest free-living relatives, the chromerids and dinoflagellates – whereas *Tg*QCR12 homologs are restricted to apicomplexans. These observations fit with an emerging narrative that mitochondria of myzozoans have evolved numerous proteins and functions that are unique amongst eukaryotes [13, 15, 35, 36]. The reasons for these novelties are unclear, but it is conceivable that the evolution of proteins like *Tg*QCR11 and *Tg*QCR12 were necessitated by evolutionary pressures for greater ETC efficiency and/or improved mitochondrial energy generation in the marine (and later parasitic) niches in which these organisms evolved. We cannot rule out the possibility that *Tg*QCR11 and *Tg*QCR12 homologs do exist in other lineages of eukaryotes, but have diverged to the extent that they can no longer be detected through even the most sophisticated homology-based searches. In future, obtaining a Complex III structure from apicomplexans will help reconcile these possibilities and shed further light on how the highly diverged and novel subunits identified in this study contribute to Complex III function.

In other eukaryotes, the small supernumerary subunits of Complex III have no well-established functions, but are hypothesized to contribute to complex stability [34]. We demonstrate that loss of *Tg*QCR11 leads to severe defects in parasite proliferation and mitochondrial oxygen consumption (Fig. 4), decreased abundance of other Complex III subunits, and the disappearance of the ~675 kDa Complex III (Fig. 6). These observations are all consistent with *Tg*QCR11 playing a critical role in maintaining Complex III integrity by mediating the assembly and/or the stability

of this complex, much like supernumerary Complex III subunits from other eukaryotes. The exact role of *Tg*QCR11 in these processes, however, remains elusive. Future functional analyses of *Tg*QCR11, including an examination of its position within the structure of Complex III, may address its actual role in the complex.

In this study, we have developed a powerful suite of assays to probe different stages and complexes of the ETC in *T. gondii* parasites. These assays rely on feeding permeabilized parasites with specific ETC substrates and inhibitors at set times during the assays. We used these assays to demonstrate that knockdown of *Tg*QCR11 caused a specific defect in Complex III function (Fig. 5), since a) the mOCR elicited by two independent substrate combinations (malate/glutamate and glycerol 3-phosphate) was decreased upon *Tg*QCR11 knockdown, and b) the fold stimulation of TMPD-dependent mOCR compared to malate/glutamate-dependent mOCR was high. This is consistent with *Tg*QCR11 functioning downstream of CoQ yet upstream of cytochrome *c* (i.e. in Complex III). By contrast, the Complex IV protein *Tg*ApiCox25 [15] had a low-fold simulation of TMPD-dependent mOCR compared to malate/glutamate-dependent mOCR, consistent with Complex IV functioning downstream of cytochrome *c* (i.e. in Complex IV). In future, these assays will enable an in-depth characterization of the function of ETC proteins and complexes, and provide a detailed understanding of the contribution of mitochondrial (and broader parasite) biosynthetic and metabolic pathways to the ETC and energy generation in these parasites. We also note that these approaches lend themselves to drug screening approaches for pin-pointing the target of ETC inhibitors in these parasites.

Our work highlights the divergence of mitochondrial ETC Complex III composition in apicomplexan parasites, providing important insights into what sets this major drug target apart

399 from the equivalent complex in host species. Future studies can now build on our findings to reveal

400 how novel subunits of this complex contribute to Complex III function and druggability.

Materials and methods

Host cell and parasite culture

T. gondii tachyzoites were cultured in human foreskin fibroblasts (HFF), as previously described [25, 37]. In paired anhydrotetracycline (ATc) knockdown experiments, ATc (0.5 µg/ml) or ethanol (vehicle control) was added to the media on required days. Plaque assays were performed as described previously [37], with 500 parasites added per flask and incubated for 7-8 days before staining with crystal violet.

Genetic modifications of T. gondii

TATiΔ*ku80* strain parasites [38] were used as the parental cell line in this study. All genetically modified parasites were cloned by flow cytometry before being characterized.

To incorporate a 3' hemagglutinin tag containing a tobacco etch virus protease cleavage site (TEV-HA tag) into the loci of *Tg*MPPα and *Tg*Cox2a, we generated a vector expressing a single guide RNA (sgRNA) targeting the region around the stop codon of *Tg*MPPα and used an existing sgRNA-expression plasmid to target *Tg*Cox2a [15]. To generate the *Tg*MPPα-targeting vector, we modified the pSAG1::Cas9-U6::sgUPRT (Addgene plasmid # 54467; [39]) vector using Q5 mutagenesis (New England Biolabs) as described previously [39]. For site-directed mutagenesis, we used the primers MPPα 3'rep CRISPR fwd and the Universal Reverse primer (Table S2). We also amplified a TEV-HA tag containing 50 bp of flanking sequence either side of the *Tg*MPPα or *Tg*Cox2a stop codon, using the primers MPPα tag fwd and MPPα tag rvs or Cox2a 3' rep fwd and Cox2a 3' rep rvs, with a TEV-HA tag template synthesized as a gBlock (IDT; Table S2). The sgRNA expressing vectors, which also expressed GFP-tagged Cas9, were co-transfected into

TATiΔ*ku80* strain parasites along with the TEV-HA tags, with transfections performed as described previously [37]. GFP-positive parasites were selected by flow cytometry and cloned 3 days following transfection, then screened for successful integration using the primers MPPα 3' screen fwd and MPPα 3' screen rvs or Cox2a 3' screen fwd and Cox2a 3' screen rvs (Table S2; Fig. S1).

To introduce 3' FLAG epitope tags into the loci of *Tg*QCR8, *Tg*QCR9, *Tg*QCR11 and *Tg*QCR12, we generated vectors expressing a sgRNA targeting the region around their stop codons. To do this, we modified the pSAG1::Cas9-U6::sgUPRT vector using Q5 mutagenesis with gene specific 3'rep CRISPR fwd primers and the Universal Reverse primer (Table S2). We also amplified a FLAG tag containing 50 bp of flanking sequence either side of the stop codon of each gene, using gene specific fwd and rvs primers, with FLAG tag template synthesized as a gBlock (IDT; Table S2). We co-transfected the plasmid and PCR product into *Tg*MPPα-HA strain parasites [18] and also into TATi/Δ*ku80* strain parasites for *Tg*QCR11, selected GFP positive parasites by flow cytometry 3 days post-transfection, then screened for successful integration using gene specific screening fwd and rvs primers (Table S2; Fig. S6; Fig. S8).

To introduce an ATc-regulated promoter into the *Tg*QCR11 locus, we generated a vector expressing a sgRNA targeting the region around the start codon of *Tg*QCR11. To do this, we modified the vector pSAG1::Cas9-U6::sgUPRT using Q5 mutagenesis with the primers QCR11 5' CRISPR fwd and the universal reverse primer (Table S2). We also PCR amplified the ATc-regulated promoter plus a 'spacer' region consisting of part of the *T. gondii* DHFR open reading frame and 3' UTR using the pPR2-HA3 vector [40] as template and the primers QCR11 pro rep fwd and QCR11 pro rep rvs (Table S2), which each contain 50 bp of sequence specific for the *Tg*QCR11 locus. We co-transfected the plasmid and the ATc-regulatable promoter into *Tg*QCR11-

445 FLAG strain parasites, selected GFP positive parasites by flow cytometry 3 days post-transfection,
446 then screened for successful integration of the ATc-regulatable promoter using the primers QCR11
447 5' screen fwd and QCR11 5' screen rvs (Table S2; Fig. S8).

448 To generate a cell line where *Tg*MPPα is HA tagged in the r*Tg*QCR11-FLAG strain, we introduced
449 a 3' HA tag to the locus of *Tg*MPPα using the vector described earlier that expresses a sgRNA
450 targeting the region around the stop codon of *Tg*MPPα. We also amplified a HA tag containing 50
451 bp of flanking sequence either side of the *Tg*MPPα stop codon, using the primers MPPα tag fwd
452 and MPPα tag rvs, with HA tag template synthesized as a gBlock (IDT; Table S2). We co-
453 transfected the plasmid and PCR product into r*Tg*QCR11-FLAG strain parasites, selected GFP
454 positive parasites by flow cytometry 3 days post-transfection, then screened for successful
455 integration using the primers MPPα 3' screen fwd and MPPα 3' screen rvs (Table S2; Fig. S8).

456 To generate a vector that constitutively expressed *Tg*QCR11 for complementing the r*Tg*QCR11
457 mutant, we ordered a gene block encoding the *Tg*QCR11 open reading frame plus a Ty1 epitope
458 tag (IDT; Table S2) and performed PCR using the primers QCR11 comp fwd and universal Ty1
459 rvs (Table S2). We digested the resulting PCR product with *Bgl*II and *Xma*I and ligated this into
460 the *Bgl*II and *Xma*I sites of the vector pUDTG (Yi Xue and G.v.D., unpublished). The resulting
461 vector contains a pyrimethamine-resistance DHFR cassette, a UPRT flanking sequence for
462 integration into the non-essential UPRT locus of *T. gondii*, and fuses a C-terminal Ty1 epitope tag
463 to the complementing *Tg*QCR11 protein. This vector was linearized in the UPRT flanking
464 sequence with *Mfe*I, transfected into r*Tg*QCR11-FLAG/*Tg*MPPα-HA parasites, and selected on
465 pyrimethamine (Sigma) as described [37].

To generate cell lines expressing either *Tg*QCR8-TEV-HA or *Tg*QCR12-TEV-HA in the r*Tg*QCR11-FLAG parasite strain, we introduced 3' TEV-HA tags into the loci of *Tg*QCR8 and *Tg*QCR12. We replicated the strategy for introducing FLAG tags into these loci that is described above, but instead co-transfected the sgRNA-expressing vectors with TEV-HA tags. We amplified TEV-HA tags containing 50 bp of flanking sequence either side of the stop codons using gene specific fwd and rvs primers, with TEV-HA tag template synthesized as a gBlock (IDT; Table S2). Following transfection, we selected GFP positive parasites by flow cytometry, then screened for successful integration using gene specific screening fwd and rvs primers (Table S2; Fig. S10).

SDS-PAGE, BN-PAGE and immunoblotting

Sodium dodecylsulfate (SDS)-polyacrylamide electrophoresis (PAGE), blue native (BN)-PAGE and immunoblotting were performed as described previously [18, 41]. Primary antibodies used included mouse anti-FLAG (1:100-1:2,000 dilution; Sigma clone M2), rat anti-HA (1:2000 dilution; Sigma clone 3F10), and rabbit anti-Tom40 (1:2,000 dilution; [18]). The secondary antibodies used were horseradish peroxidase (HRP)-conjugated goat anti-mouse IgG (Abcam), goat anti-rabbit IgG (Abcam) and goat anti-rat IgG (Abcam). For probing for mouse antibodies on immunoprecipitation western blots, HRP-conjugated anti-mouse TrueBlot ULTRA antibodies (eBioscience) were used at 1:2,500 dilution. Blots were imaged using X-ray film or using a ChemiDoc MP imaging system (BioRad).

Immunoprecipitation and mass spectrometry

Immunoprecipitations were performed as described previously [18], except that parasite samples were solubilized in 1% (v/v) Triton X-100. HA-tagged proteins were purified using anti-HA affinity matrix (Sigma; rat anti-HA clone 3F10 antibodies) and FLAG-tagged proteins were

purified using anti-FLAG M2 affinity gel (Sigma; mouse anti-FLAG clone M2 antibodies). For mass spectrometry sample preparation, parasite samples were solubilized in 1% (w/v) DDM, and processed as described previously [15]. Briefly, anti-HA affinity matrix bound with HA-tagged protein complexes were frozen at −80°C for 1 hr, then eluted at room temperature in 0.2 M glycine containing 1% (w/v) DDM (pH 2.3). Samples were neutralized in ammonium bicarbonate, then extracted in chloroform:methanol as described [42]. After extraction, the pellets were dried and stored at −80°C before mass spectrometry analysis.

Mass spectrometry was conducted as previously described [15]. Briefly, samples were resuspended in 8M Urea, 50 mM Tris pH 8.3 followed by reduction and alkylation. Solubilized proteins were submitted to trypsin digestion overnight and the resulting peptides purified using the C18 stage tips procedure. Peptides were reconstituted in 0.1% formic acid and 2% acetonitrile, loaded onto a trap column and washed for 6 min before switching the precolumn in line with the analytical column. The separation of peptides was performed as previously described (11). Data were collected on a Q Exactive HF Orbitrap mass spectrometer (Thermo-Fisher Scientific) in Data Dependent Acquisition mode using m/z 350–1500 as MS scan range at 60 000 resolution, HCD MS/MS spectra were collected for the 10 most intense ions per MS scan at 15 000 resolution with a normalized collision energy of 28% and an isolation window of 1.4 m/z. Dynamic exclusion parameters were set as follows: exclude isotope on, duration 30 s and peptide match preferred. Other instrument parameters for the Orbitrap were MS maximum injection time 30 ms with AGC target 3 × 106, MSMS for a maximum injection time of 110 ms with AGT target of 1.1 × 104. The raw data were uploaded into Peaks Studio 10.5 (Bioinformatics Solution Inc., Waterloo, Canada) and processed with de novo peptide sequencing and Peaks DB using the ToxoDB (https://toxodb.org/toxo/) database together with common contaminants (cRAP). For peptides

identification, the default settings were with precursor-ion and product-ion tolerances set to 10 ppm and 0.02 Da, respectively. Semispecific trypsin digest with a maximum of 1 missed cleavage was employed and peptides were searched with carbamidomethylation of cysteine set as fixed modification. To limit false-positive peptide identification, the false discovery rate (FDR) applied to peptide-spectrum match (PSM) was set to 1%, and at least 1 unique peptide per protein was used.

Immunofluorescence assays and microscopy

Immunofluorescence assays were performed as described previously [41]. Primary antibodies used were mouse anti-FLAG (1:500 dilution; Sigma clone M2), rat anti-HA (1:500 dilution; Sigma clone 3F10), and rabbit anti-Tom40 (1:2,000 dilution; [18]). Secondary antibodies used were goat anti-mouse Alexa Fluor 488 (1:500 dilution; Invitrogen), goat anti-rat Alexa Fluor 488 (1:500 dilution; Invitrogen), and goat anti-rabbit Alexa Fluor 546 (1:500 dilution; Invitrogen). Images were acquired on a DeltaVision Elite deconvolution microscope (GE Healthcare) fitted with a 100X UPlanSApo oil immersion objective lens (NA 1.40). Images were deconvolved and adjusted for contrast and brightness using SoftWoRx Suite 2.0 software, and subsequently processed using Adobe Illustrator.

Seahorse XFe96 extracellular flux analysis

Experiments measuring the oxygen consumption rate (OCR) and extracellular acidification rate (ECAR) of intact extracellular parasites were conducted as described previously [15, 25]. We also developed experiments to assess the OCR in digitonin-permeabilized parasites utilizing specific ETC substrates. Briefly, parasites were harvested as for the XFe96 assays on intact parasites. Parasites were then washed once in base medium (Agilent Technologies), resuspended in base

533 medium to 1.5 × 10^7 cells/mL and starved for 1 hour at 37°C to deplete endogenous ETC
534 substrates. 1.5 × 10^6 parasites were added to wells of Cell-Tak-coated Seahorse XFe96 cell culture
535 plates and adhered to the bottom by centrifugation (800 × g, 3 min). Base medium was removed
536 and replaced with 175 µL mitochondrial assay solution (MAS) buffer (220 mM mannitol, 70 mM
537 sucrose, 10 mM KH_2PO_4, 5 mM $MgCl_2$, 0.2% w/v fatty acid-free bovine serum albumin, 1 mM
538 EGTA, and 2 mM HEPES-KOH pH 7.4) containing 0.002 % (w/v) digitonin. ETC substrates and
539 inhibitors were loaded into Seahorse XFe96 sensor cartridge ports A-D, and injected into wells
540 during the experiment. OCR measurements were obtained every 3 min for five repeats before and
541 after injection of compounds (prepared in MAS buffer; concentrations given are final
542 concentrations following injection). Port A: FCCP (1 µM) plus substrates. The substrates used
543 were malate plus glutamate (10 mM each) or sn-glycerol 3-phosphate bis(cyclohexylammonium)
544 salt (G3P; 25 mM). Port B: antimycin A and atovaquone (10 µM and 1 µM, respectively). Port C:
545 N,N,N′,N′-tetramethyl-p-phenylenediamine dihydrochloride (TMPD; 0.2 mM) mixed with
546 ascorbic acid (3.3 mM). Port D: sodium azide (NaN_3; 10 mM). Substrate-elicited mOCR was
547 calculated by subtracting the non-mitochondrial OCR (the values following antimycin A and
548 atovaquone injection via Port B) from the OCR value obtained after substrate injection (Port A).
549 Likewise, TMPD-elicited mOCR was calculated by subtracting the non-mitochondrial OCR from
550 the OCR value obtained after TMPD injection (Port C). A minimum of 4 background wells were
551 used in each plate, and 3 technical replicates were used for each condition.

552 ***Data analyses and availability***

553 Data from the Seahorse flux analysis were exported from the Seahorse Wave Desktop software
554 (Agilent Technologies). A linear mixed effects model was applied to the data as described
555 previously [15], setting the error between plates (between experiments) and wells (within

556 experiments) as random effects, and the mOCR or ECAR values between cell lines and days on
557 drug (ATc) as fixed effects. Analysis of the least square means of the values was performed in the
558 R software environment. Statistical differences between these values were tested through ANOVA
559 (linear mixed effects), with a post hoc Tukey test.

560 Data from the *Tg*MPPα-TEV-HA and *Tg*Cox2a-TEV-HA mass spectrometry-based proteomic
561 experiment were analyzed in the R software environment using the EdgeR package as described
562 previously [15, 43]. In the analysis performed to produce the volcano plot, only proteins identified
563 in both data sets and each biological replicate were included, while subsequent analyses also
564 considered proteins that were absent from one or more replicates of the *Tg*Cox2a-TEV-HA control.

565 The mass spectrometry proteomics data have been deposited to the ProteomeXchange consortium
566 via the Pride partner repository [44] with the dataset identified PXD018781 and
567 10.6019/PXD018781.

568 ***Bioinformatic analyses***

569 Amino acid sequences of *T. gondii* Complex III proteins were accessed from ToxoDB
570 (www.toxodb.org). Initial identification of homologs in the apicomplexan parasites *P. falciparum*
571 and *C. parvum,* and the chromerids *V. brassicaformis* and *C. velia,* was performed through Basic
572 Local Alignment Search Tool (tBLASTn) searches of the EuPathDB Transcripts database
573 (www.eupathdb.org., [45]). Where simple BLAST searches did not identify homologs, additional
574 homology searches were performed using the iterative search tool JackHMMER
575 (www.ebi.ac.uk/Tools/hmmer/search/jackhmmer) and the profile hidden Markov model based
576 search tool HHPRED (https://toolkit.tuebingen.mpg.de/tools/hhpred, [23]). To identify homologs
577 of *Tg*QCR8 and *Tg*QCR9 in yeast, humans, *Arabidopsis* and the parasitic dinoflagellate *Perkinsus*

578 *marinus*, we performed JackHMMER and NCBI iterative PSI-BLAST [46] searches. We
579 identified dinoflagellate homologs of *Tg*QCR8, *Tg*QCR9 and *Tg*QCR11 using BLAST searches
580 of *Symbiodinium* spp. genomes available at http://reefgenomics.org [47]. Transmembrane domain
581 predictions were performed using TMHMM [48] and TMPred (https://embnet.vital-
582 it.ch/software/TMPRED_form.html). Multiple protein sequence alignments of QCR8 (Fig. S2),
583 QCR9 (Fig. S3), *Tg*QCR11 (Fig. S4) and *Tg*QCR12 (Fig. S5) were performed using Clustal Omega
584 [49], and the graphical output was generated in BoxShade (https://embnet.vital-
585 it.ch/software/BOX_form.html). All accession numbers are included in the supplementary figure
586 legends.

587 **Acknowledgements**

588 We thank Harpreet Vohra and Michael Devoy (ANU) for assistance with flow cytometry, Michael
589 Devoy for assistance with establishing the XFe96 assays, Teresa Neeman from the ANU Statistical
590 Consulting Unit for assistance with data analysis, the ANU Toxo lab for comments on the
591 manuscript, and the 2019 ANU Cell Biology course for contributing to the generation of parasite
592 strains. We are grateful to EuPathDB for providing numerous datasets and search tools.

References

1. Wang JL, Zhang NZ, Li TT, He JJ, Elsheikha HM, Zhu XQ. Advances in the Development of Anti-*Toxoplasma gondii* Vaccines: Challenges, Opportunities, and Perspectives. Trends Parasitol. 2019;35(3):239-53. Epub 2019/02/06. doi: 10.1016/j.pt.2019.01.005. PubMed PMID: 30718083.
2. King A. Building a better malaria vaccine. Nature. 2019;575(7784):S51-s4. Epub 2019/11/30. doi: 10.1038/d41586-019-03639-5. PubMed PMID: 31776499.
3. Goodman CD, Buchanan HD, McFadden GI. Is the Mitochondrion a Good Malaria Drug Target? Trends Parasitol. 2017;33(3):185-93. Epub 2016/10/30. doi: 10.1016/j.pt.2016.10.002. PubMed PMID: 27789127.
4. Mather MW, Henry KW, Vaidya AB. Mitochondrial drug targets in apicomplexan parasites. Curr Drug Targets. 2007;8(1):49-60. Epub 2007/02/03. PubMed PMID: 17266530.
5. Alday PH, Doggett JS. Drugs in development for toxoplasmosis: advances, challenges, and current status. Drug Des Devel Ther. 2017;11:273-93. Epub 2017/02/10. doi: 10.2147/DDDT.S60973. PubMed PMID: 28182168; PubMed Central PMCID: PMCPMC5279849.
6. Doggett JS, Nilsen A, Forquer I, Wegmann KW, Jones-Brando L, Yolken RH, et al. Endochin-like quinolones are highly efficacious against acute and latent experimental toxoplasmosis. Proc Natl Acad Sci U S A. 2012;109(39):15936-41. doi: 10.1073/pnas.1208069109. PubMed PMID: 23019377; PubMed Central PMCID: PMC3465437.
7. Srivastava IK, Morrisey JM, Darrouzet E, Daldal F, Vaidya AB. Resistance mutations reveal the atovaquone-binding domain of cytochrome *b* in malaria parasites. Mol Microbiol. 1999;33(4):704-11. PubMed PMID: 10447880.
8. Mitchell P. The protonmotive Q cycle: a general formulation. FEBS Lett. 1975;59(2):137-9. Epub 1975/11/15. PubMed PMID: 1227927.
9. Yoshikawa S, Shimada A. Reaction mechanism of cytochrome *c* oxidase. Chem Rev. 2015;115(4):1936-89. Epub 2015/01/21. doi: 10.1021/cr500266a. PubMed PMID: 25603498.
10. Santo-Domingo J, Demaurex N. The renaissance of mitochondrial pH. Journal of General Physiology. 2012;139(6):415-23. doi: 10.1085/jgp.201110767.
11. Hayward JA, van Dooren GG. Same same, but different: Uncovering unique features of the mitochondrial respiratory chain of apicomplexans. Mol Biochem Parasitol. 2019;232:111204. Epub 2019/08/06. doi: 10.1016/j.molbiopara.2019.111204. PubMed PMID: 31381948.
12. Flegontov P, Michalek J, Janouskovec J, Lai DH, Jirku M, Hajduskova E, et al. Divergent mitochondrial respiratory chains in phototrophic relatives of apicomplexan parasites. Mol Biol Evol. 2015;32(5):1115-31. doi: 10.1093/molbev/msv021. PubMed PMID: 25660376.
13. Barylyuk K, Koreny L, Ke H, Butterworth S, Crook OM, Lassadi I, et al. A subcellular atlas of *Toxoplasma* reveals the functional context of the proteome. bioRxiv preprint. 2020. doi: 10.1101/2020.04.23.057125.
14. Salunke R, Mourier T, Banerjee M, Pain A, Shanmugam D. Highly diverged novel subunit composition of apicomplexan F-type ATP synthase identified from *Toxoplasma gondii*. PLoS Biol. 2018;16(7):e2006128. Epub 2018/07/14. doi: 10.1371/journal.pbio.2006128. PubMed PMID: 30005062; PubMed Central PMCID: PMCPMC6059495.
15. Seidi A, Muellner-Wong LS, Rajendran E, Tjhin ET, Dagley LF, Aw VY, et al. Elucidating the mitochondrial proteome of *Toxoplasma gondii* reveals the presence of a divergent cytochrome c oxidase. Elife. 2018;7:e38131. Epub 2018/09/12. doi: 10.7554/eLife.38131. PubMed PMID: 30204084; PubMed Central PMCID: PMCPMC6156079.

16. Huet D, Rajendran E, van Dooren GG, Lourido S. Identification of cryptic subunits from an apicomplexan ATP synthase. eLife. 2018;7:e38097. Epub 2018/09/12. doi: 10.7554/eLife.38097. PubMed PMID: 30204085; PubMed Central PMCID: PMCPMC6133553.
17. Roger AJ, Munoz-Gomez SA, Kamikawa R. The Origin and Diversification of Mitochondria. Curr Biol. 2017;27(21):R1177-R92. Epub 2017/11/08. doi: 10.1016/j.cub.2017.09.015. PubMed PMID: 29112874.
18. van Dooren GG, Yeoh LM, Striepen B, McFadden GI. The Import of Proteins into the Mitochondrion of *Toxoplasma gondii*. J Biol Chem. 2016;291(37):19335-50. doi: 10.1074/jbc.M116.725069. PubMed PMID: 27458014.
19. Glaser E, Eriksson A, Sjoling S. Bifunctional role of the bc1 complex in plants. Mitochondrial bc1 complex catalyses both electron transport and protein processing. FEBS Lett. 1994;346(1):83-7. Epub 1994/06/06. doi: 10.1016/0014-5793(94)00312-2. PubMed PMID: 8206164.
20. McFadden DC, Tomavo S, Berry EA, Boothroyd JC. Characterization of cytochrome *b* from *Toxoplasma gondii* and Q(o) domain mutations as a mechanism of atovaquone-resistance. Mol Biochem Parasitol. 2000;108(1):1-12. Epub 2000/05/10. PubMed PMID: 10802314.
21. Ossorio PN, Sibley LD, Boothroyd JC. Mitochondrial-like DNA sequences flanked by direct and inverted repeats in the nuclear genome of *Toxoplasma gondii*. J Mol Biol. 1991;222(3):525-36. Epub 1991/12/05. doi: 10.1016/0022-2836(91)90494-q. PubMed PMID: 1660924.
22. Seeber F, Limenitakis J, Soldati-Favre D. Apicomplexan mitochondrial metabolism: a story of gains, losses and retentions. Trends Parasitol. 2008;24(10):468-78. doi: 10.1016/j.pt.2008.07.004. PubMed PMID: 18775675.
23. Zimmermann L, Stephens A, Nam SZ, Rau D, Kubler J, Lozajic M, et al. A Completely Reimplemented MPI Bioinformatics Toolkit with a New HHpred Server at its Core. J Mol Biol. 2018;430(15):2237-43. Epub 2017/12/21. doi: 10.1016/j.jmb.2017.12.007. PubMed PMID: 29258817.
24. Sidik SM, Huet D, Ganesan SM, Huynh MH, Wang T, Nasamu AS, et al. A Genome-wide CRISPR Screen in *Toxoplasma* Identifies Essential Apicomplexan Genes. Cell. 2016;166(6):1423-35.e12. Epub 2016/09/07. doi: 10.1016/j.cell.2016.08.019. PubMed PMID: 27594426; PubMed Central PMCID: PMCPMC5017925.
25. Tjhin ET, Hayward JA, McFadden GI, van Dooren GG. Characterization of the apicoplast-localized enzyme *Tg*UroD in *Toxoplasma gondii* reveals a key role of the apicoplast in heme biosynthesis. J Biol Chem. 2020;295(6):1539-50. Epub 2020/01/09. doi: 10.1074/jbc.RA119.011605. PubMed PMID: 31914409.
26. Salabei JK, Gibb AA, Hill BG. Comprehensive measurement of respiratory activity in permeabilized cells using extracellular flux analysis. Nat Protoc. 2014;9(2):421-38. doi: 10.1038/nprot.2014.018. PubMed PMID: 24457333; PubMed Central PMCID: PMCPMC4063296.
27. Vercesi AE, Rodrigues CO, Uyemura SA, Zhong L, Moreno SN. Respiration and oxidative phosphorylation in the apicomplexan parasite *Toxoplasma gondii*. J Biol Chem. 1998;273(47):31040-7. PubMed PMID: 9813002.
28. Iwata S, Lee JW, Okada K, Lee JK, Iwata M, Rasmussen B, et al. Complete structure of the 11-subunit bovine mitochondrial cytochrome bc1 complex. Science. 1998;281(5373):64-71. Epub 1998/07/04. doi: 10.1126/science.281.5373.64. PubMed PMID: 9651245.
29. Xia D, Yu CA, Kim H, Xia JZ, Kachurin AM, Zhang L, et al. Crystal structure of the cytochrome bc1 complex from bovine heart mitochondria. Science. 1997;277(5322):60-6. Epub 1997/07/04. doi: 10.1126/science.277.5322.60. PubMed PMID: 9204897.
30. Zhang Z, Huang L, Shulmeister VM, Chi YI, Kim KK, Hung LW, et al. Electron transfer by domain movement in cytochrome bc1. Nature. 1998;392(6677):677-84. Epub 1998/05/16. doi: 10.1038/33612. PubMed PMID: 9565029.

31. Hunte C, Koepke J, Lange C, Rossmanith T, Michel H. Structure at 2.3 A resolution of the cytochrome bc(1) complex from the yeast *Saccharomyces cerevisiae* co-crystallized with an antibody Fv fragment. Structure. 2000;8(6):669-84. Epub 2000/06/30. doi: 10.1016/s0969-2126(00)00152-0. PubMed PMID: 10873857.
32. Meyer EH, Taylor NL, Millar AH. Resolving and identifying protein components of plant mitochondrial respiratory complexes using three dimensions of gel electrophoresis. J Proteome Res. 2008;7(2):786-94. Epub 2008/01/15. doi: 10.1021/pr700595p. PubMed PMID: 18189341.
33. Zara V, Conte L, Trumpower BL. Identification and characterization of cytochrome bc_1 subcomplexes in mitochondria from yeast with single and double deletions of genes encoding cytochrome bc_1 subunits. FEBS J. 2007;274(17):4526-39. Epub 2007/08/08. doi: 10.1111/j.1742-4658.2007.05982.x. PubMed PMID: 17680808.
34. Xia D, Esser L, Tang WK, Zhou F, Zhou Y, Yu L, et al. Structural analysis of cytochrome bc_1 complexes: implications to the mechanism of function. Biochim Biophys Acta. 2013;1827(11-12):1278-94. Epub 2012/12/04. doi: 10.1016/j.bbabio.2012.11.008. PubMed PMID: 23201476; PubMed Central PMCID: PMCPMC3593749.
35. Danne JC, Gornik SG, Macrae JI, McConville MJ, Waller RF. Alveolate mitochondrial metabolic evolution: dinoflagellates force reassessment of the role of parasitism as a driver of change in apicomplexans. Mol Biol Evol. 2013;30(1):123-39. doi: 10.1093/molbev/mss205. PubMed PMID: 22923466.
36. Jacot D, Waller RF, Soldati-Favre D, MacPherson DA, MacRae JI. Apicomplexan Energy Metabolism: Carbon Source Promiscuity and the Quiescence Hyperbole. Trends Parasitol. 2016;32(1):56-70. Epub 2015/10/17. doi: 10.1016/j.pt.2015.09.001. PubMed PMID: 26472327.
37. Jacot DL, S.; Markus, M.; Sheiner, L.; Soldati-Favre, D.; Striepen, B. Genetic manipulation of *Toxoplasma gondii*. In: Weiss LMK, K. , editor. *Toxoplasma gondii* the model apicomplexan - perspectives and methods. Third edition ed. London: Academic Press; 2020. p. 897-934.
38. Sheiner L, Demerly JL, Poulsen N, Beatty WL, Lucas O, Behnke MS, et al. A systematic screen to discover and analyze apicoplast proteins identifies a conserved and essential protein import factor. PLoS Pathog. 2011;7(12):e1002392. doi: 10.1371/journal.ppat.1002392. PubMed PMID: 22144892.
39. Shen B, Brown KM, Lee TD, Sibley LD. Efficient gene disruption in diverse strains of *Toxoplasma gondii* using CRISPR/CAS9. MBio. 2014;5(3):e01114-14. doi: 10.1128/mBio.01114-14. PubMed PMID: 24825012; PubMed Central PMCID: PMCPMC4030483.
40. Katris NJ, van Dooren GG, McMillan PJ, Hanssen E, Tilley L, Waller RF. The apical complex provides a regulated gateway for secretion of invasion factors in *Toxoplasma*. PLoS Pathog. 2014;10(4):e1004074. doi: 10.1371/journal.ppat.1004074. PubMed PMID: 24743791; PubMed Central PMCID: PMC3990729.
41. van Dooren GG, Tomova C, Agrawal S, Humbel BM, Striepen B. *Toxoplasma gondii* Tic20 is essential for apicoplast protein import. Proc Natl Acad Sci U S A. 2008;105(36):13574-9. Epub 2008/09/02. doi: 10.1073/pnas.0803862105. PubMed PMID: 18757752; PubMed Central PMCID: PMCPMC2533231.
42. Pankow S, Bamberger C, Calzolari D, Bamberger A, Yates JR, 3rd. Deep interactome profiling of membrane proteins by co-interacting protein identification technology. Nat Protoc. 2016;11(12):2515-28. doi: 10.1038/nprot.2016.140. PubMed PMID: 27854364; PubMed Central PMCID: PMCPMC5444904.
43. Robinson MD, Smyth GK. Small-sample estimation of negative binomial dispersion, with applications to SAGE data. Biostatistics. 2008;9(2):321-32. doi: 10.1093/biostatistics/kxm030. PubMed PMID: 17728317.
44. Perez-Riverol Y, Csordas A, Bai J, Bernal-Llinares M, Hewapathirana S, Kundu DJ, et al. The PRIDE database and related tools and resources in 2019: improving support for quantification data.

Nucleic Acids Res. 2019;47(D1):D442-d50. Epub 2018/11/06. doi: 10.1093/nar/gky1106. PubMed PMID: 30395289; PubMed Central PMCID: PMCPMC6323896.

45. Aurrecoechea C, Barreto A, Basenko EY, Brestelli J, Brunk BP, Cade S, et al. EuPathDB: the eukaryotic pathogen genomics database resource. Nucleic Acids Res. 2017;45(D1):D581-d91. Epub 2016/12/03. doi: 10.1093/nar/gkw1105. PubMed PMID: 27903906; PubMed Central PMCID: PMCPMC5210576.

46. Altschul SF, Madden TL, Schaffer AA, Zhang J, Zhang Z, Miller W, et al. Gapped BLAST and PSI-BLAST: a new generation of protein database search programs. Nucleic Acids Res. 1997;25(17):3389-402. PubMed PMID: 9254694.

47. Liew YJ, Aranda M, Voolstra CR. Reefgenomics.Org - a repository for marine genomics data. Database (Oxford). 2016;2016. Epub 2016/12/28. doi: 10.1093/database/baw152. PubMed PMID: 28025343; PubMed Central PMCID: PMCPMC5199144.

48. Krogh A, Larsson B, von Heijne G, Sonnhammer EL. Predicting transmembrane protein topology with a hidden Markov model: application to complete genomes. J Mol Biol. 2001;305(3):567-80. Epub 2001/01/12. doi: 10.1006/jmbi.2000.4315. PubMed PMID: 11152613.

49. Sievers F, Higgins DG. Clustal Omega for making accurate alignments of many protein sequences. Protein Sci. 2018;27(1):135-45. Epub 2017/09/09. doi: 10.1002/pro.3290. PubMed PMID: 28884485; PubMed Central PMCID: PMCPMC5734385.

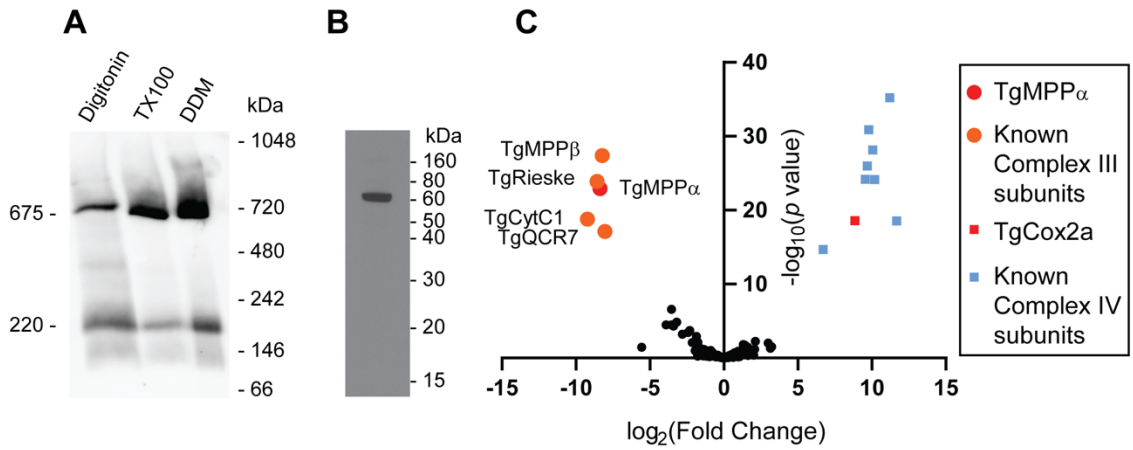

D

	ID	Annotation	PS	Mass (kDa)	Mito Proteome	"LOPIT"	Homology Pf	Vb	Cv	Cp
known	TGGT1_236210	TgQCR1/TgMPPβ	-4.74	56.915	y	MM				
known	TGGT1_320220	TgRieske	-5.76	54.791	y	MM				
known	TGGT1_202680	TgQCR2/TgMPPα	-4.30	62.203	y	MM				
known	TGGT1_288750	TgQCR7/14 kDa	-4.04	26.741	y	MM				
known	TGGT1_246540	TgCytC1	-4.36	45.968	y	MM				
known	TGGT1_320140	TgQCR6/Hinge	-3.69	10.493	y	MM				
known	TGGT1_362110	TgCytB homolog	N/A	10.376	N/A	N/A				
novel	TGGT1_201880	TgQCR9*	-3.68	15.269	y	MM				
novel	TGGT1_227910	TgQCR8*	-3.20	14.373	y	MM				
novel	TGGT1_207170	TgQCR12	-3.44	15.231	y	MM	#			
novel	TGGT1_214250	TgQCR11	-3.94	9.444	y	O, MM				
	TGGT1_270800	GAF protein	-0.29	83.924	y	MM				
	TGGT1_242780	Hypothetical	-3.85	427.75	n	N, PM				

*HHPred; #JackHMMR

<5 >150

$-\log_{10}$(E-value)

Fig 1: *Tg*MPPα is part of a ~675 kDa protein complex and co-purifies with known components of Complex III. (A) Western blot of proteins extracted from *Tg*MPPα-TEV-HA parasites in 1% (w/v) digitonin, 1% (v/v) TX100 or 1% (w/v) DDM-containing lysis buffer, separated by BN-PAGE, and detected with anti-HA antibodies. **(B)** Western blot of proteins extracted from *Tg*MPPα-TEV-HA parasites, separated by SDS-PAGE, and detected with anti-HA antibodies. **(C)** Volcano plot showing the $\log_2$ fold change vs $-\log_{10}$ *p* values of proteins purified from *Tg*MPPα-TEV-HA vs *Tg*Cox2a-TEV-HA parasites using anti-HA immunoprecipitations and detected by mass spectrometry. To enable statistical comparisons, only proteins detected in all

three independent experiments for both parasite lines are depicted. Proteins enriched in the *Tg*MPPα-TEV-HA samples ($p < 0.05$; $\log_2$ fold change > 5) are labelled and shown in orange circles, with *Tg*MPPα shown in red. Similarly, proteins previously identified as *T. gondii* Complex IV subunits [15] are shown in blue squares, with *Tg*Cox2a shown in red. **(D)** Table summarising the characteristics of proteins identified in proteomic analysis of the *Tg*MPPα-TEV-HA complex (modelled after [16]). Proteins with homology to Complex III proteins are shown in orange circles, novel or divergent Complex III proteins are depicted by green circles, and proteins identified in the initial proteomic analysis but excluded in subsequent analyses are depicted in gray circles. Protein IDs were obtained from ToxoDB and proposed annotations are listed. The phenotype score (PS) of each gene predicts its importance for parasite proliferation, with scores < -2 typically found in genes that are important for proliferation [24]. Detection in the mitochondrial proteome (Mito Proteome, [15]) and its predicted cellular localisation ("LOPIT" [13]) are indicated (y = yes, n = no, N/A = not available, MM = mitochondrial membranes, O = outlier, N = nucleus, PM = plasma membrane). Homology indicates the tBLASTn expected value (E-value) between each *T. gondii* protein sequence and its closest match in *Plasmodium falciparum* (Pf), *Vitrella brassicaformis* (Vb), *Chromera velia* (Cv) or *Cryptosporidium parvum* (Cp) using EuPathDB searches. Black circles indicate a close match could not be identified. *, homology detected using HHPRED; #, homology detected using iterative JackHMMER searches.

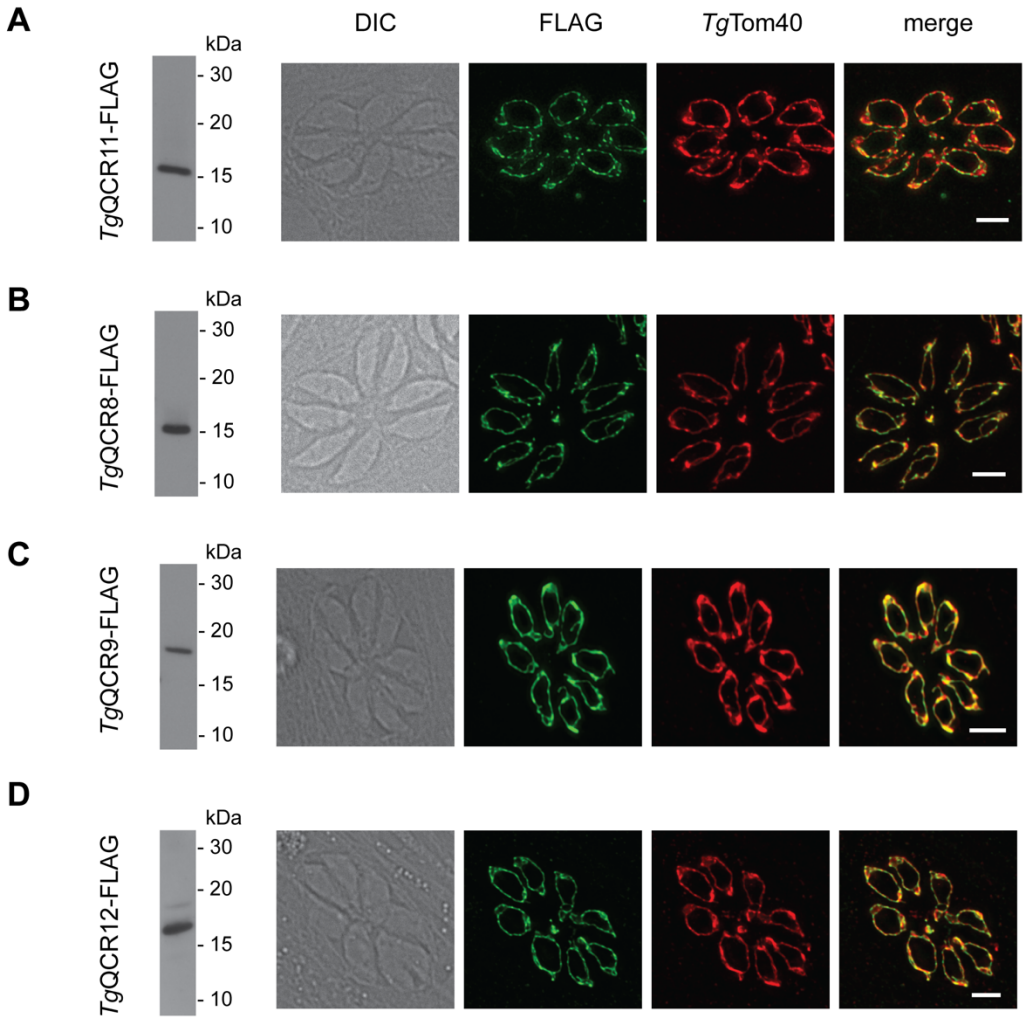

778

779 **Fig 2: Candidate Complex III subunits localize to the mitochondrion of *T. gondii*.** (Left)
780 Western blot and (Right) immunofluorescence assay analysis of **(A)** *Tg*MPPα-HA/*Tg*QCR11-
781 FLAG, **(B)** *Tg*MPPα-HA/*Tg*QCR8-FLAG, **(C)** *Tg*MPPα-HA/*Tg*QCR9-FLAG, or **(D)** *Tg*MPPα-
782 HA/*Tg*QCR12-FLAG parasites. Western blots were detected with anti-FLAG antibodies, and
783 immunofluorescence assays were detected with anti-FLAG (green) and the mitochondrial marker
784 anti-*Tg*Tom40 (red) antibodies. Scale bars represent 2 μm.

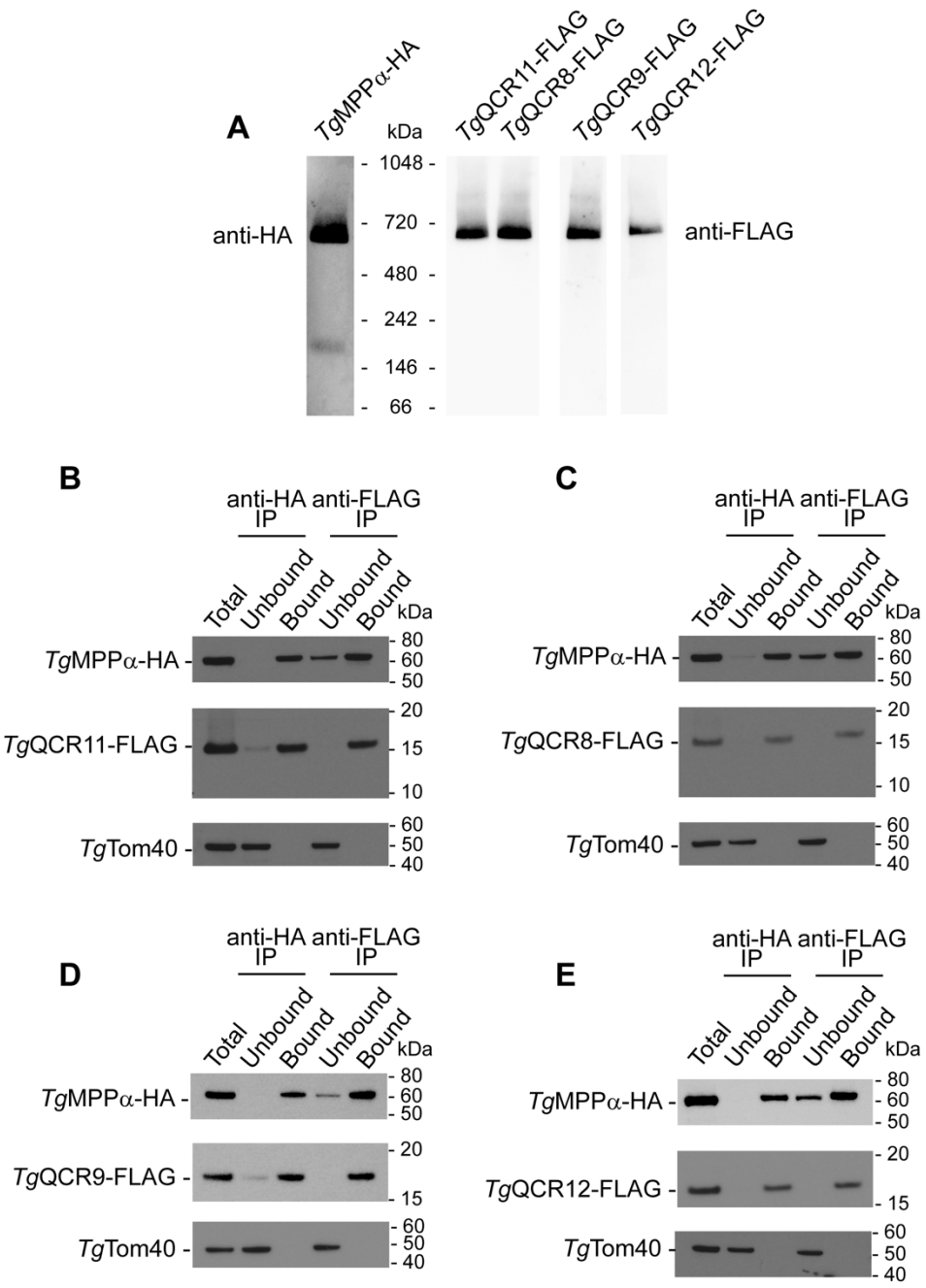

Fig 3: Candidate Complex III subunits are part of a ~675 kDa protein complex and interact with *Tg*MPPα. (A) Western blot of proteins extracted from *Tg*MPPα-TEV-HA (left) or *Tg*MPPα-HA/*Tg*QCR11-FLAG, *Tg*MPPα-HA/*Tg*QCR8-FLAG, *Tg*MPPα-HA/*Tg*QCR9-FLAG and *Tg*MPPα-HA/*Tg*QCR12-FLAG parasites in 1% (w/v) DDM, separated by BN-PAGE, and detected with anti-HA or anti-FLAG antibodies. Images were obtained from proteins transferred

to a single membrane, with lanes cut as indicated and probed with different concentration of antibodies. **(B-E)** Western blots of proteins extracted from **(B)** *Tg*MPPα-HA/*Tg*QCR11-FLAG, **(C)** *Tg*MPPα-HA/*Tg*QCR8-FLAG, **(D)** *Tg*MPPα-HA/*Tg*QCR9-FLAG or **(E)** *Tg*MPPα-HA/*Tg*QCR12-FLAG parasites, and subjected to immunoprecipitation using anti-HA (anti-HA IP) or anti-FLAG (anti-FLAG IP) antibody-coupled beads. Extracts include samples before immunoprecipitation (Total), samples that did not bind to the anti-HA or anti-FLAG beads (Unbound), and samples that bound to the anti-HA or anti-FLAG beads (Bound). Samples were separated by SDS-PAGE, and probed with anti-HA antibodies to detect *Tg*MPPα-HA, anti-FLAG to detect *Tg*QCRs, and anti-*Tg*Tom40 as a control to detect an unrelated mitochondrial protein.

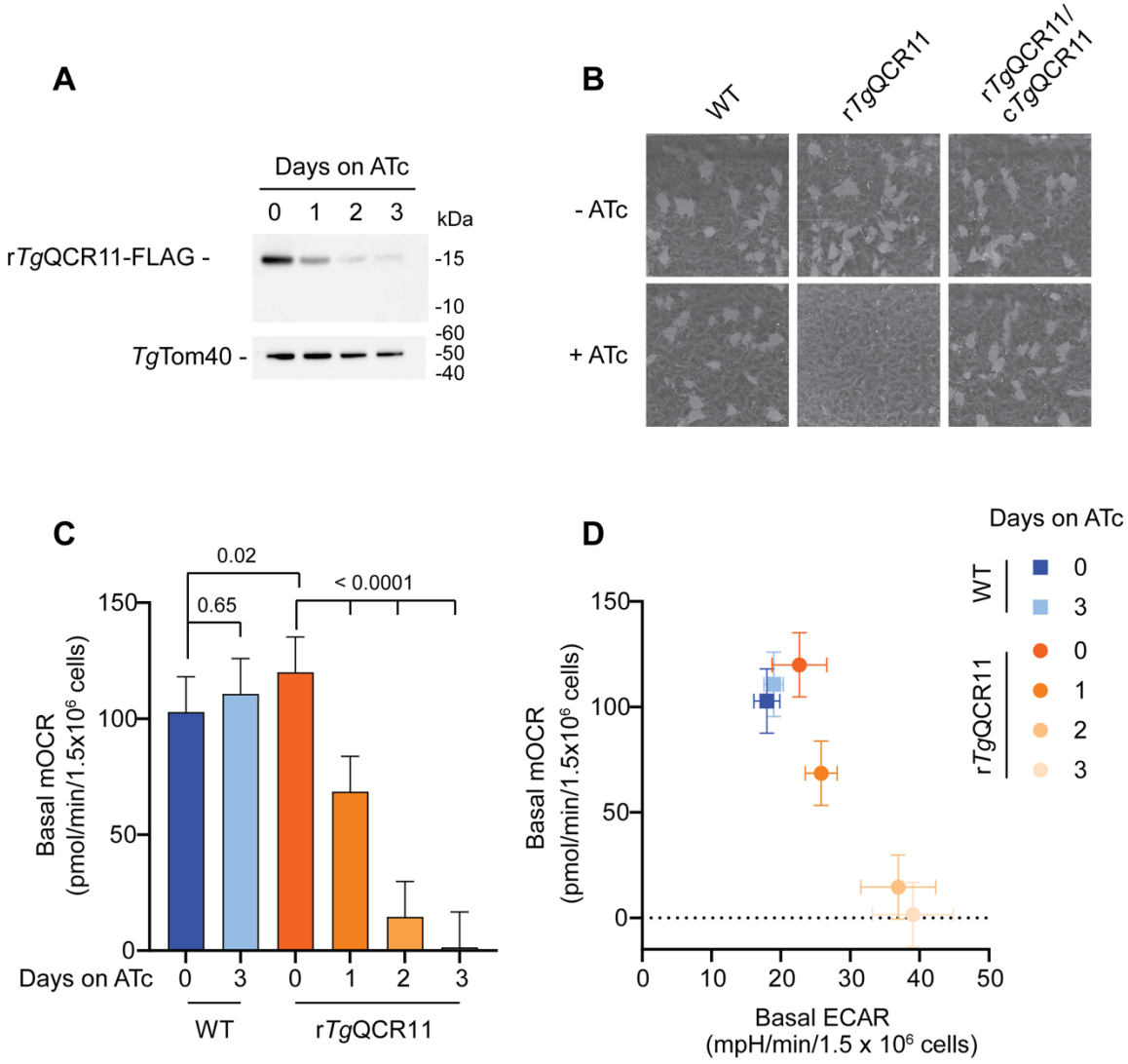

Fig 4: The apicomplexan-specific Complex III subunit *Tg*QCR11 is important for parasite proliferation and mitochondrial oxygen consumption. (A) Western blot of proteins extracted from r*Tg*QCR11-FLAG/*Tg*MPPα-HA parasites grown in the absence of ATc, or in the presence of ATc for 1-3 days, separated by SDS-PAGE, and detected using anti-FLAG and anti-*Tg*Tom40 antibodies (loading control). **(B)** Plaque assays measuring growth of WT, r*Tg*QCR11-FLAG/*Tg*MPPα-HA and complemented c*Tg*QCR11-Ty1/r*Tg*QCR11-FLAG/*Tg*MPPA-HA parasites cultured in the absence (top) or presence (bottom) of ATc for 8 days. Assays are from a single experiment and are representative of 3 independent experiments. **(C)** Basal mitochondrial

809 oxygen consumption rates (mOCR) of extracellular WT parasites grown in the absence of ATc or
810 in the presence of ATc for 3 days (blue), and r*Tg*QCR11-FLAG/*Tg*MPPA-HA parasites grown in
811 the absence of ATc or in the presence of ATc for 1-3 days (orange). A linear mixed-effects model
812 was fitted to the data and values depict the least squares mean ± 95% CI of three independent
813 experiments. ANOVA followed by Tukey's multiple pairwise comparisons test was performed,
814 with relevant *p* values shown. **(D)** Basal mOCR versus basal extracellular acidification rate
815 (ECAR) of WT parasites grown in the absence of ATc or in the presence of ATc for 3 days (blue),
816 and r*Tg*QCR11-FLAG/*Tg*MPPA-HA parasites grown in the absence of ATc or in the presence of
817 ATc for 1-3 days (orange). Data depict the mean mOCR and ECAR values ± 95% CI of the linear
818 mixed-effects model (n = 3).

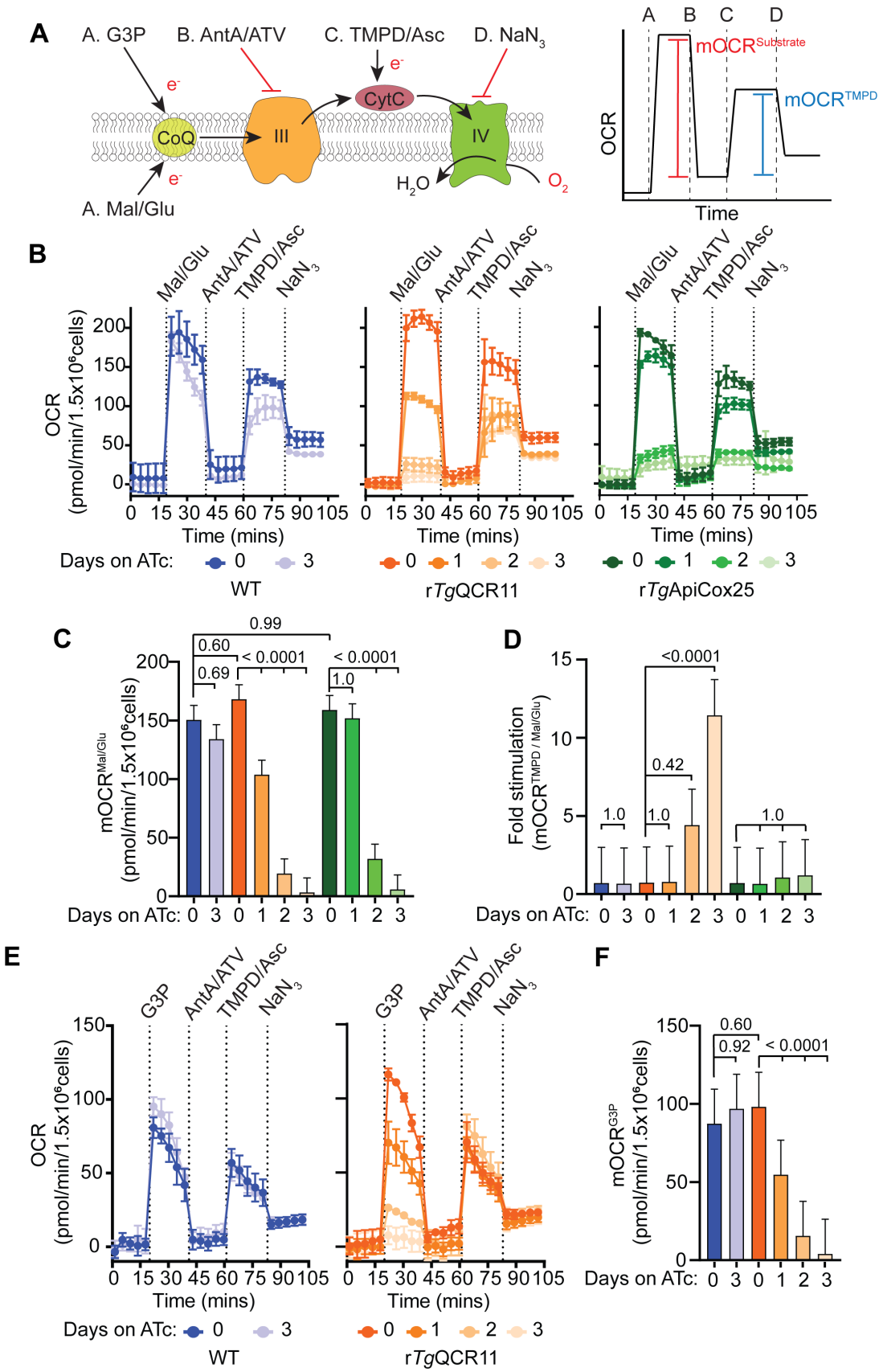

819

Fig 5: Loss of *Tg*QCR11 leads to a specific defect in Complex III function. (A) Schematic diagram of the assay measuring OCR in extracellular digitonin-permeabilized parasites, with inset (right) depicting a mock oxygen consumption rate (OCR) versus time graph to illustrate the typical response of WT parasites. Parasites are starved for 1 hour in base media to deplete endogenous energy sources, then permeabilized with 0.002% (w/v) digitonin before being subjected to the following injections of substrates or inhibitors: Port A, malate and glutamate (Mal/Glu) or glycerol 3-phopshate (G3P); Port B, antimycin A and atovaquone (AntA/ATV); Port C, TMPD and ascorbate (TMPD/Asc); Port D, sodium azide (NaN_3). The mitochondrial OCR (mOCR) elicited by a substrate (red line, $mOCR^{substrate}$) and the mOCR elicited by TMPD/Asc (blue line, $mOCR^{TMPD}$) are then calculated from these data. CytC, cytochrome *c*; CoQ, coenzyme Q; III, Complex III; IV, Complex IV; e^-, electrons. **(B)** Representative traces depicting OCR over time when supplying Mal/Glu (10 mM) as an energy source. WT (blue), r*Tg*QCR11-FLAG/*Tg*MPPα-HA (orange) and r*Tg*ApiCox25-HA (green) parasites were grown in the absence of ATc or in the presence of ATc for 1-3 days. Data represent the mean ± SD of three technical replicates, and are representative of three independent experiments. **(C)** Mal/Glu elicited mOCR ($mOCR^{Mal/Glu}$) of WT (blue), r*Tg*QCR11-FLAG/*Tg*MPPα-HA (orange) and r*Tg*ApiCox25-HA (green) parasites that were grown in the absence of ATc or in the presence of ATc for 1-3 days. A linear mixed-effects model was fitted to the data and values depict the least squares mean ± 95% CI from three independent experiments. ANOVA followed by Tukey's multiple pairwise comparisons test was performed, with relevant *p* values shown. **(D)** Fold stimulation of mOCR by TMPD relative to Mal/Glu in WT (blue), r*Tg*QCR11-FLAG/*Tg*MPPα-HA (orange) and r*Tg*ApiCox25-HA (green) parasites that had been grown in the absence of ATc or in the presence of ATc for 1-3 days (mean ± 95% CI of the linear mixed-effects model; n = 3). ANOVA followed by Tukey's multiple

pairwise comparisons test was performed, with relevant *p* values shown. **(E)** Representative traces depicting OCR over time when supplying the TCA-independent substrate G3P (10 mM) as an energy source. WT (blue) and r*Tg*QCR11-FLAG/*Tg*MPPα-HA (orange) parasites were grown in the absence of ATc or in the presence of ATc for 1-3 days. Data represent the mean ± SD of three technical replicates, and are representative of three independent experiments. **(F)** G3P elicited mOCR ($mOCR^{G3P}$) of WT (blue) and r*Tg*QCR11-FLAG/*Tg*MPPα-HA (orange) parasites that were grown in the absence of ATc or in the presence of ATc for 1-3 days (mean ± 95% CI of the linear mixed-effects model; n = 3). ANOVA followed by Tukey's multiple pairwise comparisons test was performed, with relevant *p* values shown.

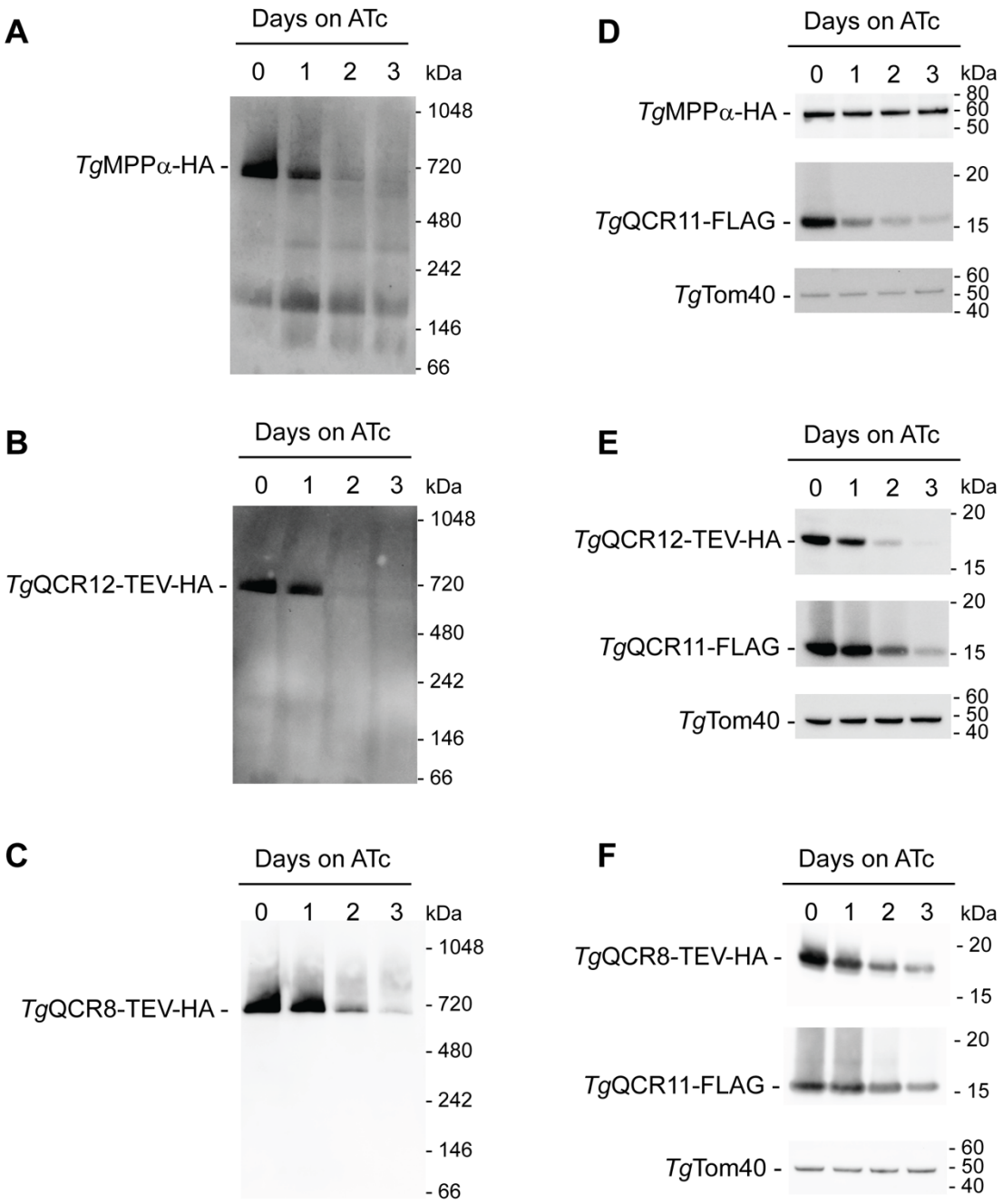

852

853 **Fig 6: *Tg*QCR11 is important for Complex III integrity. (A-C)** Western blots of proteins
854 extracted from **(A)** r*Tg*QCR11-FLAG/*Tg*MPPα-HA, **(B)** r*Tg*QCR11-FLAG/*Tg*QCR12-TEV-HA,
855 and **(C)** r*Tg*QCR11-FLAG/*Tg*QCR8-TEV-HA parasites that had been grown in the absence of
856 ATc or in the presence of ATc for 1-3 days. Samples were prepared in 1% (w/v) DDM, separated

by BN-PAGE, and detected with anti-HA antibodies. **(D-F)** Western blots of proteins extracted from **(D)** r*Tg*QCR11-FLAG/*Tg*MPPα-HA, **(E)** r*Tg*QCR11-FLAG/*Tg*QCR12-TEV-HA, and **(F)** r*Tg*QCR11-FLAG/*Tg*QCR8-TEV-HA parasites that had been grown in the absence of ATc or in the presence of ATc for 1-3 days. Samples were separated by SDS-PAGE, and probed with anti-HA, anti-FLAG and anti-*Tg*Tom40 (loading control) antibodies. Western blots shown are representative of at least two independent experiments, with matched BN-PAGE and SDS-PAGE samples prepared from the same experiment.